Original Article

ENO2 promotes anoikis resistance in anaplastic thyroid cancer by maintaining redox homeostasis

Yu Zhang[1,2#], Xiaoyu Ji[3#], Yu Wang[1,2]

[1]Department of Head and Neck Surgery, Fudan University Shanghai Cancer Center, Shanghai, China; [2]Department of Oncology, Shanghai Medical College, Fudan University, Shanghai, China; [3]Department of Oncology, Huashan Hospital, Fudan University, Shanghai, China

Contributions: (I) Conception and design: Y Wang; (II) Administrative support: Y Wang; (III) Provision of study materials or patients: Y Zhang; (IV) Collection and assembly of data: Y Zhang; (V) Data analysis and interpretation: X Ji; (VI) Manuscript writing: All authors; (VII) Final approval of manuscript: All authors.

[#]These authors contributed equally to this work.

Correspondence to: Yu Wang, MD, PhD. Department of Head and Neck Surgery, Fudan University Shanghai Cancer Center, Shanghai, China; Department of Oncology, Shanghai Medical College, Fudan University, No. 270 Dong'An Rd, Xuhui District, Shanghai 200030, China. Email: neck130@sina.com.

Background: Anoikis presents a significant barrier in the metastasis of cancer. As the most aggressive type of thyroid cancer, anaplastic thyroid cancer (ATC) exhibits a high risk of metastasis and is characterized by high mortality. Therefore, investigating the molecular mechanisms of anoikis resistance in ATC is important for devising therapeutic targets in clinical research.

Methods: Differentially Expressed Genes were screened in ATC cells under attached and detached culture conditions with RNA-seq. Investigate the impact of enolase 2 (ENO2) on apoptosis and spheroid formation by gain and loss of function. Changes of reactive oxygen species (ROS), glutathione (GSH) and nicotinamide adenine dinucleotide phosphate (NADPH) were detected to assess redox balance. The transcriptional regulatory role of signal transducer and activator of transcription 1 (STAT1) on ENO2 was validated through Dual-Luciferase Reporter Gene Assay. Explore the impact of ENO2 expression on the formation of lung metastases in nude mice.

Results: We found that the glycolysis process was activated in detached ATC cells. Several genes in the glycolysis process, particularly *ENO2*, a member of the enolase superfamily was upregulated in ATC cells cultured in suspension. The upregulation of ENO2 enabled the maintenance of redox balance by supplying GSH and NADPH, thereby preventing cells from undergoing anoikis. In terms of mechanism, the expression of STAT1 was enhanced in anoikis resistance cells, which in turn positively regulated the expression of ENO2. *In vivo*, ENO2-suppressed ATC cells resulted in a significantly lower rate of lung colonization compared to control ATC cells.

Conclusions: Stable expression of ENO2 and the maintenance of redox balance played a pivotal role in facilitating anoikis resistance of ATC.

Keywords: Anoikis resistance; metastasis; enolase 2 (ENO2); redox homeostasis; anaplastic thyroid cancer (ATC)

Submitted Feb 01, 2024. Accepted for publication Feb 15, 2024. Published online Feb 23, 2024.
doi: 10.21037/gs-24-44
View this article at: https://dx.doi.org/10.21037/gs-24-44

Introduction

Patients with differentiated thyroid cancer generally have a favorable prognosis; however, those with undifferentiated thyroid cancers, including poorly differentiated thyroid cancer (PDTC) and anaplastic thyroid cancer (ATC), have an extremely poor prognosis (1-5). Despite the relatively low incidence of ATC among thyroid cancers, it represents a significant cause of mortality in thyroid cancer patients,

leading to serious therapeutic challenges (6). Patients often present with local and distant metastases at the time of the initial diagnosis, revealing the urgent need for further research into the mechanisms of metastasis in ATC (7,8).

Metastasis often leads to deadly outcomes in cancer (9). Current research indicates that the cells of primary sites may go through multiple steps to gain the ability to invade surrounding tissues and enter circulation (10). However, to accomplish eventual colonization in distant organs, the cells' fate in circulation is particularly important. Anoikis is defined as the apoptosis that occurs when cells detach from the surrounding extracellular matrix (ECM) (11-14). After detaching from the primary lesions, the majority of tumor cells are eliminated through this process; however, a small subset of cancer cells reprogram intracellular and extracellular signals to survive in lymphatic and blood vessels (15,16). However, the role of anoikis resistance in ATC cells remains unknown and is worthy of further research.

The Warburg effect observed in cancer cells can be described as an altered metabolic preference where these cells favor heightened glucose consumption and predominantly use glycolysis for energy production, even when oxygen is available (17,18). Further, instead of channeling pyruvate (the end product of glycolysis) into the mitochondrial oxidation pathway, cancer cells tend to convert it to lactate (17). This diversion aids in preventing the excessive production of reactive oxygen species (ROS), helping cancer cells to maintain a more reduced cellular environment (19). This alteration allows the cells to evade a process called anoikis, which is a form of programmed cell death induced by detachment from the ECM (20).

Enolase 2 (ENO2), also known as human neuron-specific enolase or γ-enolase, is one of the rate-limiting enzymes in glycolysis, facilitating the conversion of 2-phosphoglycerate to phosphoenolpyruvate (21,22). It serves as a general marker in cell differentiation in neuroendocrine tumors and has been noted to be a well-established tumor biomarker in various types of cancers, including prostate cancer, small-cell lung cancer, and the microvascular invasion status of liver cancer (23-25). Several studies have suggested that ENO2 contributes to metastasis by stimulating glycolytic activity (26-28). The forced expression of oncogenes rescues the anoikis of mammary epithelial cells by increasing glucose utilization and decreasing oxidative stress levels (29). Huang reported that hexokinase 2 (HK2), an enzyme that plays a key role in glycolysis-supported cell survival by facilitating glycolysis, subsequently decreases excessive ROS levels (30). Meanwhile, Jin revealed that the activation of lactate dehydrogenase A via phosphorylation, an enzyme responsible for converting pyruvate to lactate, stimulates cancer cell invasion, anoikis resistance, and the spread of tumors to distant sites (31).

In this study, through transcriptomic sequencing, the glycolytic pathway was found to be significantly activated in ATC cells under detached culture conditions. We also identified ENO2 as a potential promising target for modulating energy homeostasis and anoikis resistance in ATC cells. By manipulating ENO2 expression, we observed a profound reversal of anoikis resistance both *in vitro* and *in vivo*. This reversal was achieved by disrupting the supply of nicotinamide adenine dinucleotide phosphate (NADPH) and glutathione (GSH), thereby disturbing the redox balance. Further, we found that the detached culture condition could induce the upregulation of ENO2 through the increased expression of the transcription factor signal transducer and activator of transcription 1 (STAT1). Our findings highlight the significant role of ENO2-mediated glycolysis in anoikis resistance and suggest that ENO2 could be a novel therapeutic target for ATC metastasis. We present this article in accordance with the ARRIVE and MDAR reporting checklists (available at https://gs.amegroups.com/article/view/10.21037/gs-24-44/rc).

Highlight box

Key findings

- Enolase 2 (ENO2) promotes anoikis resistance in anaplastic thyroid cancer (ATC).

What is known and what is new?

- The activated glycolysis process in anoikis-resistant cancer cells is a well-known factor in the occurrence of metastasis in ATC.
- We demonstrated that the upregulation of ENO2 facilitates the maintenance of redox balance, while the newly identified function of enhanced transcription by STAT1 contributes to anoikis resistance in ATC.

What is the implication, and what should change now?

- Anoikis resistance is a crucial therapeutic target for ATC.
- Targeting ENO2 to inhibit metastasis in ATC is worth further exploration.

Methods

Tissue samples and cell lines

Human ATC cell lines (8305C, SW1736, and C643)

were purchased from the cell bank of Chinese Academy of Sciences (Shanghai, China). The cells were cultured in Dulbecco's Modified Eagle Medium (Gibco, Logan, UT, USA) containing 10% fetal bovine serum, supplemented with 100 IU/mL of penicillin and streptomycin (Gibco, New York, NY, USA). Tissue samples of poorly differentiated and ATC patients at the Fudan University Shanghai Cancer Center (FUSCC, Shanghai, China) were collected between January 2010 and December 2019. The study was conducted in accordance with the Declaration of Helsinki (as revised in 2013). The study was approved by the Ethics Committee of Fudan University Shanghai Cancer Center (No. 050432-4-2108) and informed consent was taken from all the patients.

Reagents and antibodies

N-acetyl-L-cysteine (NAC, HY-B0215) was purchased from MedChemExpress (Monmouth, NJ, USA). Annexin V-FITC and PI kit apoptosis detection kit was obtained from BD (Franklin Lakes, NJ, USA). 2',7'-dichlorofluorescin diacetate (DCF-DA) was acquired from Beyotime (Shanghai, China). The following antibodies were used for the western blot analysis: α-tubulin (ab52866, Abcam, Cambridge, UK), GAPDH (60004-1-Ig, Proteintech, Wuhan, China), ENO2 (10149-1-AP proteintech, Wuhan, China), STAT1 (10144-2-AP, Proteintech), PARP1 (13371-1-AP, Proteintech), and H2AX (10856-1-AP, Proteintech).

Plasmid transfection and RNA interference

The ENO2 knockdown and overexpression lentiviral construction systems were obtained from Genechem (Shanghai, China). The ATC cells were stably transfected with ENO2 knockdown and overexpression lentiviruses along with the corresponding control plasmids to confer puromycin resistance. In accordance with the manufacturer's instructions, stable transfections were selected using puromycin (2 μg/mL) for 2–3 days to generate stable ENO2 knockdown and overexpression cell lines. The sequence of the short hairpin RNA (*ENO2*) was 5'-GCCGGACATAACTTCCGTAAT-3' and 5'-GGTCCAAGTTCACAGCCAATG-3'. *STAT1* gene (*STAT1*-siRNA1 CTGTGATGTTAGATAAACA, *STAT1*-siRNA2 GCAGCACAACATACGGAAA) and negative control (NC) were synthesized by Biotend Co., Ltd. (Shanghai, China). The cells were transfected with 50 nM of small interfering RNA for 24 hours using the jetPRIME transfection kit (Polyplus-transfection, Strasbourg, France).

Total RNA extraction, reverse transcription, and quantitative real-time polymerase chain reaction (qRT-PCR)

Total RNA extraction was conducted using TRIzol reagent (Invitrogen, Waltham, MA, USA) in accordance with the manufacturer's instructions. RNA purity and concentration were assessed using the NanoDrop2000 spectrophotometer. Total RNA (1 μg) was reverse transcribed using the PrimeScript RT reagent kit (Takara, Dalian, China). For the qRT-PCR, complementary DNA was amplified using SYBR Green Premix Ex Taq (Takara, Dalian, China) in accordance with the manufacturer's instructions. Gene expression was normalized to β-actin messenger RNA (mRNA) expression and relative mRNA expression levels were determined using the comparative Ct ($2^{-\Delta\Delta Ct}$) method. The primer sequences used are listed in *Table 1*.

Western blotting

The cultured cells were washed with ice-cold phosphate-buffered saline (PBS) before the total cell protein lysates were extracted at 4 ℃ for 30 minutes using RIPA Lysis Buffer (Beyotime) containing a 1% protease inhibitor cocktail (MedChemExpress). After centrifugation with 12,000 g for 20 minutes at 4 ℃, the supernatant was collected and mixed with loading buffer, and boiled at 100 ℃ in a metal bath for 10 minutes. The samples were subjected to 10% sodium dodecyl-sulfate polyacrylamide gel electrophoresis separation, and then transferred onto a polyvinylidene fluoride (PVDF) membrane. After blocking with 5% skimmed milk for 2 hours at room temperature, the PVDF membrane was then incubated in primary antibodies overnight at 4 ℃. Subsequently, the PVDF membrane was incubated with secondary antibodies after being washed with Tris Buffered Saline with Tween. The PVDF membrane was eventually detected with enhanced chemiluminescence reagents (Beyotime). The primary antibodies were as follows: α-tubulin (1:5,000), GAPDH (1:5,000), ENO2 (1:1,000), STAT1 (1:1,000), PARP1 (1:1,000), and H2AX (1:1,000). The secondary antibodies were as follows: anti-rabbit secondary antibody (1:3,000), anti-mouse secondary antibody (1:3,000).

Table 1 Primers used for qRT-PCR

Gene	Forward (5'-3')	Reverse (5'-3')
β-actin	TGACGTGGACATCCGCAAAG	CTGGAAGGTGGACAGCGAGG
ALDOA	ATGCCCTACCAATATCCAGCA	GCTCCCAGTGGACTCATCTG
LDHA	ATGGCAACTCTAAAGGATCAGC	CCAACCCCAACAACTGTAATCT
PGK1	GAACAAGGTTAAAGCCGAGCC	GTGGCAGATTGACTCCTACCA
ENO2	AGGTGCAGAGGTCTACCATAC	AGCTCCAAGGCTTCACTGTTC
SLC2A1	TCTGGCATCAACGCTGTCTTC	CGATACCGGAGCCAATGGT
SLC2A3	GCTGGGCATCGTTGTTGGA	GCACTTTGTAGGATAGCAGGAAG
STAT1	ATCAGGCTCAGTCGGGGAATA	TGGTCTCGTGTTCTCTGTTCT

qRT-PCR, quantitative reverse transcription polymerase chain reaction.

Immunohistochemistry (IHC) assays

After deparaffinization, the paraffin sections were incubated with 3% hydrogen peroxide at 26 ℃ for 10 minutes to suppress endogenous peroxidase activity. Following blocking with 10% goat serum, the sections were incubated overnight at 4 ℃ with primary antibodies. Subsequently, the sections were incubated with horse radish peroxidase-conjugated rabbit secondary antibodies for 1 hour at room temperature, and then underwent DAB staining. The staining results were calculated based on the percentage of the cell nuclei stained (0: no staining, 1: <10%, 2: 10–50%, and 3: >50%) and the staining intensity (0: negative, 1: weak positive, 2: moderate positive, 3: strong positive). The overall score was the product of these two scores. An overall score of 1–3 indicated a low expression of ENO2, while a score of 4–9 indicated a high expression of ENO2.

RNA-sequencing data analysis

Total RNA (5 milligrams per sample) was extracted from the 8305C, SW1736, and C643 cell lines cultured in adherent and low-attachment conditions. Paired-end sequencing was conducted using Illumina Hiseq 150PE by GENEWIZ Limited (Suzhou, China). A gene set enrichment analysis (GSEA) was performed based on the RNA-sequencing data.

Luciferase reporter assays

The luciferase reporter gene analysis was conducted using the Dual-Luciferase Reporter Assay System (Promega, Madison, WI, USA). The human *ENO2* promoter sequence and its mutated counterpart were separately inserted into the pGL3 basic vector. The constructed pGL3-*ENO2*-promoter plasmids and the Renilla luciferase control plasmid were co-transfected into the cells. Luciferase activity was measured at 72 hours post-transfection. Normalization of the reporter gene activity was performed using Renilla luciferase.

Chromatin immunoprecipitation assays

Chromatin immunoprecipitation assays were performed using the Simple ChIP Enzymatic Chromatin IP Kit (Magnetic Beads, Cell Signaling Technology, #9003). Briefly, the 8305C cells were cross-linked with 1% formaldehyde at room temperature for 10 minutes. Following sonication, the cell lysates were used to shear chromatin DNA into fragments (between 200 and 500 bp in size). The chromatin supernatant was then incubated with an equal amount of anti-STAT1 or anti-immunoglobulin G antibody. The incubation was carried out overnight at 4 ℃ with rotation. After de-crosslinking the protein/DNA complexes, qRT-PCR was performed using specific primers (forward primer: 5'-ACACCTGTCAGTTTCTACAGA-3', reverse primer: 5'-CATTATTCAGAGAGAGCAGTGG-3') to detect the immunoprecipitated DNA.

Assessment of anoikis and sphere formation assays

The cell death of the ATC cells cultured in the detached culture condition was determined using the Annexin V/PI kit (BD). The cells were cultured on ultra-low attachment plates for specific period and trypsinized to generate a single-cell suspension before the flow cytometry analysis. For anchorage-independent growth, the cells were

cultured in serum-free medium, supplemented with 20 ng/mL of epidermal growth factor (100-47, Peprotech, Pittsburgh, PA, USA), 20 ng/mL of basic fibroblast growth factor (100-18B, Peprotech), 10 µg/mL of heparin (H3149, Sigma, St. Louis, MO, USA), and 2% B27 (17504044, Gibco). Subsequently, the number of spheres formed in each well was observed and measured under a microscope after 5 days.

Measurement of cellular ROS

To measure the ROS levels within the cells, the ATC cells were collected and trypsinized to generate a single-cell suspension. Subsequently, the cells were stained with 1 µM of DCF-DA. After incubation at 37 ℃ for 30 minutes, the cells were washed twice with PBS before the flow cytometry analysis.

Detection of the cellular NADPH/NADP+ and GSH/GSSG ratios

The cellular levels of NADPH/$NADP^+$ were determined by the WST-8 method using the NADPH/$NADP^+$ assay kit (S0179, Beyotime). In brief, approximately 1×10^6 cells were lysed using the NADPH/$NADP^+$ extraction solution. Around 200 µL of the test sample was transferred to a centrifuge tube and heated at 60 ℃ in a water bath for 30 minutes to decompose $NADP^+$ (if the total NADPH/$NADP^+$ was being measured, this step was omitted). Subsequently, 50 µL of the supernatant was added to a 96-well plate and mixed with G6PDH working solution and incubated at 37 ℃ in the dark for 10 minutes. The coloring reagent was added and absorbance was measured at 450 nm. Quantification was performed based on a standard curve.

The cellular GSH/GSSG was measured using the GSH and GSSG assay kit (S0053, Beyotime) in accordance with the manufacturer's instructions. Briefly, the cells were collected and re-suspended in protein removal reagent M, immediately vortexed for 10 seconds, and subjected to two cycles of freezing and thawing using liquid nitrogen and a 37 ℃ water bath. After incubation for 5 minutes at 4 ℃, the samples were centrifuged at 10,000 ×g for 10 minutes at 4 ℃. The resulting supernatant was reacted with DTNB [5,5'-dithiobis (2-nitrobenzoic acid)], GSH reductase, and NADPH to generate a yellow-colored TNB (5'-thio-2-nitrobenzoic acid), which was measured for absorbance at 412 nm. Quantification was performed based on standard curves.

In vivo metastasis assays

The nude mouse lung metastasis tumor model was created through the random assignment of all nude mice into two groups (of eight mice per group). This randomization process was done using a simple randomization method. In total, 8305C cells (1×10^6), expressing shCtrl or shENO2, were injected via the tail vein into female BABL/c nude mice (3–4 weeks old) purchased from GemPharmatech (Nanjing, China). After six weeks, the mice were euthanized, and their lungs were excised painlessly. All micrometastases were examined using a dissecting microscope after staining with hematoxylin and eosin. Animal experiments were performed under a project license (No. FUSCC-IACUC-S2023-0429) granted by Experimental Animal Welfare Ethics Committee of Fudan University Shanghai Cancer Center, in compliance with institutional guidelines for the care and use of animals. A protocol was prepared before the study without registration.

Statistical analysis

The provided data are presented as the mean ± standard deviation (SD). All the experiments were repeated at least three times. The statistical analysis was conducted using GraphPad Prism 7 (San Diego, CA, USA) and SPSS ver.19.0 (SPSS Inc., Chicago, IL, USA). The Student's *t*-test was used to compare the continuous variables. The Mann-Whitney *U*-test was used to compare the continuous data with a non-normal distribution. The clinical characteristics were compared using the chi-square. Fisher's exact tests was used to compare the categorical variables. A P value <0.05 was considered statistically significant.

Results

ENO2 was induced in detached ATC cells and increased in metastatic lymph nodes compared with the primary tumor sites

To imitate the detached culture conditions of ATC cells in the circulatory system, the ATC cell lines SW1736, 8305C, and C643 were cultured on ultra-low attachment plates. After 48 hours, a transcriptomic analysis was conducted on the SW1736, 8305C, and C643 cells cultured under both adherent and low-attachment conditions (*Figure 1A*). The GSEA revealed significant activation of the glycolysis pathway (*Figure 1B*). Among the six genes showing an upregulated trend in all three cell lines, *ENO2* exhibited a

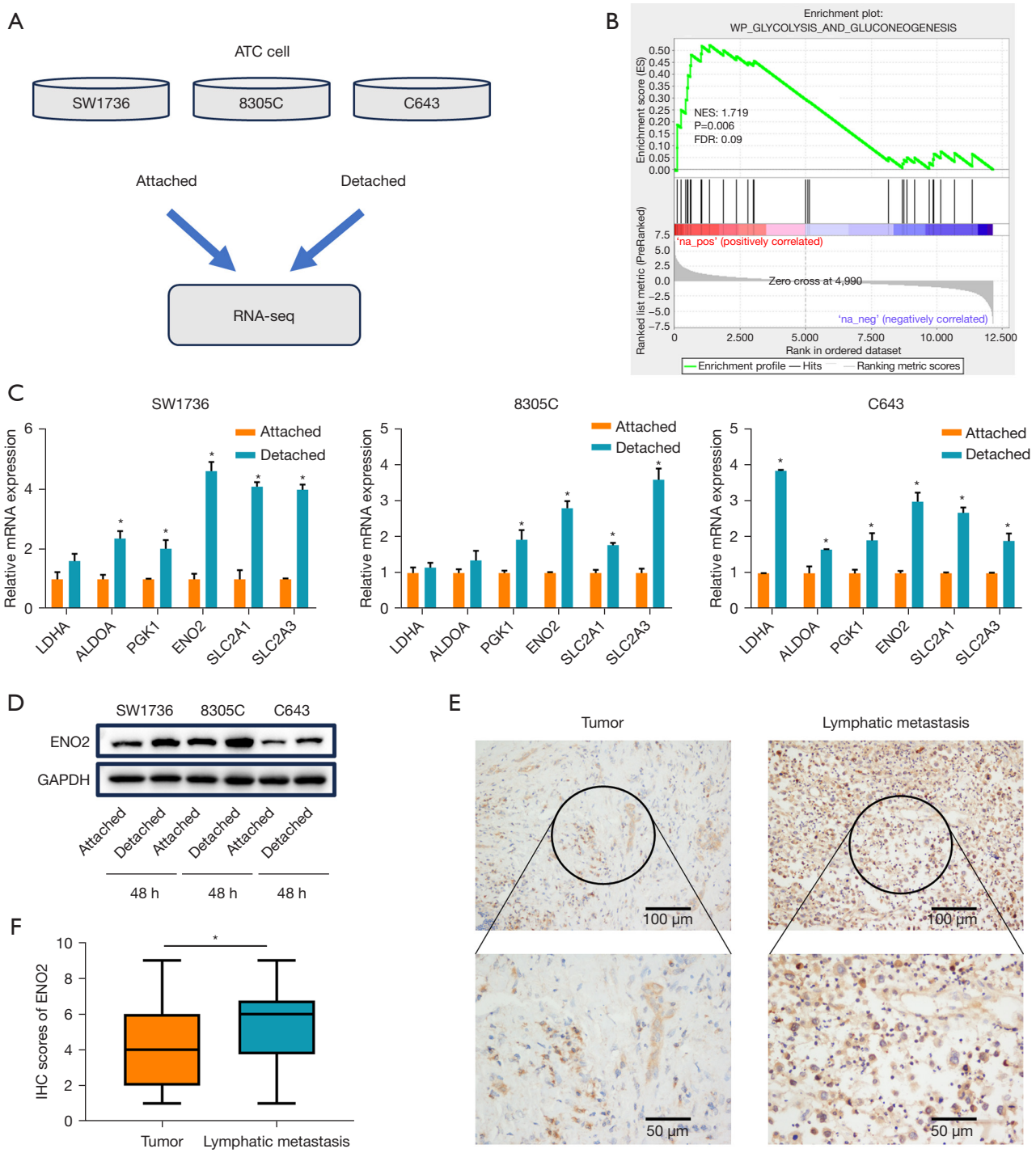

Figure 1 ENO2 expression was elevated in ATC cells upon detachment, and ENO2 levels were higher in metastatic lymph nodes than primary tumor sites. (A) Illustration depicting the strategy employed in the transcriptome analysis comparing the ATC cells under the attached and detached culture conditions. (B) The GSEA showed that the glycolysis pathway was significantly activated and the amino acid metabolism pathway was significantly inactivated in the detached cells. (C) The mRNA levels of several glycolysis-related genes, including *LDHA*, *ALDOA*, *PGK1*, *ENO2*, *SLC2A1*, and *SLC2A3* were analyzed in the attached and detached SW1736, 8305C, and C643 cells. (D) Western blot analysis of ENO2 expression in the SW1736, 8305C, and C643 cells in the attached and detached culture conditions for 2 days. (E) Representative IHC staining images of ENO2. (F) The IHC staining scores of the ENO2 levels in the primary tumor sites and the metastatic lymph nodes of the ATC tissues from FUSCC (N=42). The data in C are expressed as the mean ± standard deviation. The data in F are depicted in a box-and-whisker graph (minimum–maximum), where the horizontal line in each box represents the median value. The P values in C and F were calculated using the Student's *t*-test (two-sided paired or unpaired). *, P<0.05. ENO2, enolase 2; ATC, anaplastic thyroid cancer; GSEA, Gene Set Enrichment Analysis; NES, Normalized Enrichment Score; FDR, false discovery rate; mRNA, messenger RNA; IHC, Immunohistochemistry; FUSCC, Fudan University Shanghai Cancer Center.

Table 2 Correlation of ENO2 expression with clinicopathological characteristics in ATC/PDTC patients of the FUSCC

Variables	Low (n=28)	High (n=29)	P value
Gender			0.678
Female	17 (51.52%)	16 (48.48%)	
Male	11 (45.83%)	13 (54.17%)	
Age, years			0.713
<55	11 (52.38%)	10 (47.62%)	
≥55	17 (47.22%)	19 (52.78%)	
ETE			0.906
Yes	15 (48.39%)	16 (51.61%)	
No	13 (50.00%)	13 (50.00%)	
Multifocality or unifocal			0.523
Multifocal	11 (55.00%)	9 (45.00%)	
Unifocal	17 (45.95%)	20 (54.05%)	
Coexistent HT			0.372
Yes	4 (66.67%)	2 (33.33%)	
No	24 (47.06%)	27 (52.94%)	
Bilateral			0.941
Unilateral	21 (48.84%)	22 (51.16%)	
Bilateral	7 (50.00%)	7 (50.00%)	
T stage			0.930
T1–T2	9 (50.00%)	9 (50.00%)	
T3–T4	19 (48.72%)	20 (51.28%)	
LNM			0.029*
N0	11 (73.33%)	4 (26.67%)	
N1	17 (40.48%)	25 (59.52%)	
Distant metastasis			0.131
M0	20 (57.14%)	15 (42.86%)	
M1	8 (36.36%)	14 (63.64%)	

*, P<0.05 is considered statistically significant. ENO2, enolase 2; ATC, anaplastic thyroid cancer; PDTC, poorly differentiated thyroid cancer; FUSCC, Fudan University Shanghai Cancer Center; ETE, extrathyroidal extension; HT, Hashimoto's thyroiditis; LNM, lymph node metastasis.

consistently significant increase, as further confirmed by the qRT-PCR analysis (*Figure 1C*). Consequently, we chose *ENO2* for further research. The western blotting results confirmed that the expression of ENO2 was more elevated in the SW1736, 8305C, and C643 cells in the detached culture conditions than in the adherent culture conditions (*Figure 1D*).

Subsequently, we assessed the expression of ENO2 via IHC in primary cancer lesions and metastatic cervical lymph nodes (*Figure 1E*). The data indicated that the levels of ENO2 expression were significantly higher in the metastatic lymph nodes than in the paired primary tumors (*Figure 1F*). Meanwhile, the correlation of ENO2 with the clinicopathological characteristics of the PDTC/ATC patients in the FUSCC was analyzed (*Table 2*). High ENO2 expression was significantly associated with lymph node metastasis (LNM), such that ENO2 was more highly expressed in patients more likely to have LNM. The combined cellular and ICH results indicate that elevated ENO2 levels may contribute to the survival and formation of metastases in ATC cells in the circulatory system.

ENO2 regulated anoikis resistance in ATC cells

To further examine the role of ENO2 in the metastasis of ATCs, we observed its effect on anoikis by knocking down and overexpressing ENO2 in the three ATC cell lines. The SW1736 and 8305C cell lines with relatively high levels of ENO2 expression were selected to construct the knockdown cell lines, while the C643 cell line was selected for ENO2 overexpression (*Figure 1D*). Knockdown efficiency was assessed by western blotting (*Figure 2A*). ENO2 knockdown induced a significant proportion of cell apoptosis in the SW1736 and 8305C cells cultured under the detached culture condition, while the cells cultured under adherent condition remained viable regardless of ENO2 expression (*Figure 2B*,*2C*). Additionally, the sphere formation numbers, which represented the anchorage-independent growth, were significantly inhibited by ENO2 knockdown in the SW1736 and 8305C cells in the detached culture condition (*Figure 2D*,*2E*). Finally, we overexpressed ENO2 in the C643 cells and validated the results by western blotting (*Figure 2F*). ENO2 overexpression significantly suppressed cell apoptosis and promoted sphere formation under the detached culture condition (*Figure 2G-2I*). The anoikis was further confirmed by western blot analysis of PARP1 and H2AX in both the ENO2 knockdown and overexpression cells under the detached culture condition (*Figure 2J*). Thus, ENO2 was essential for the survival of ATC cells under the detached condition.

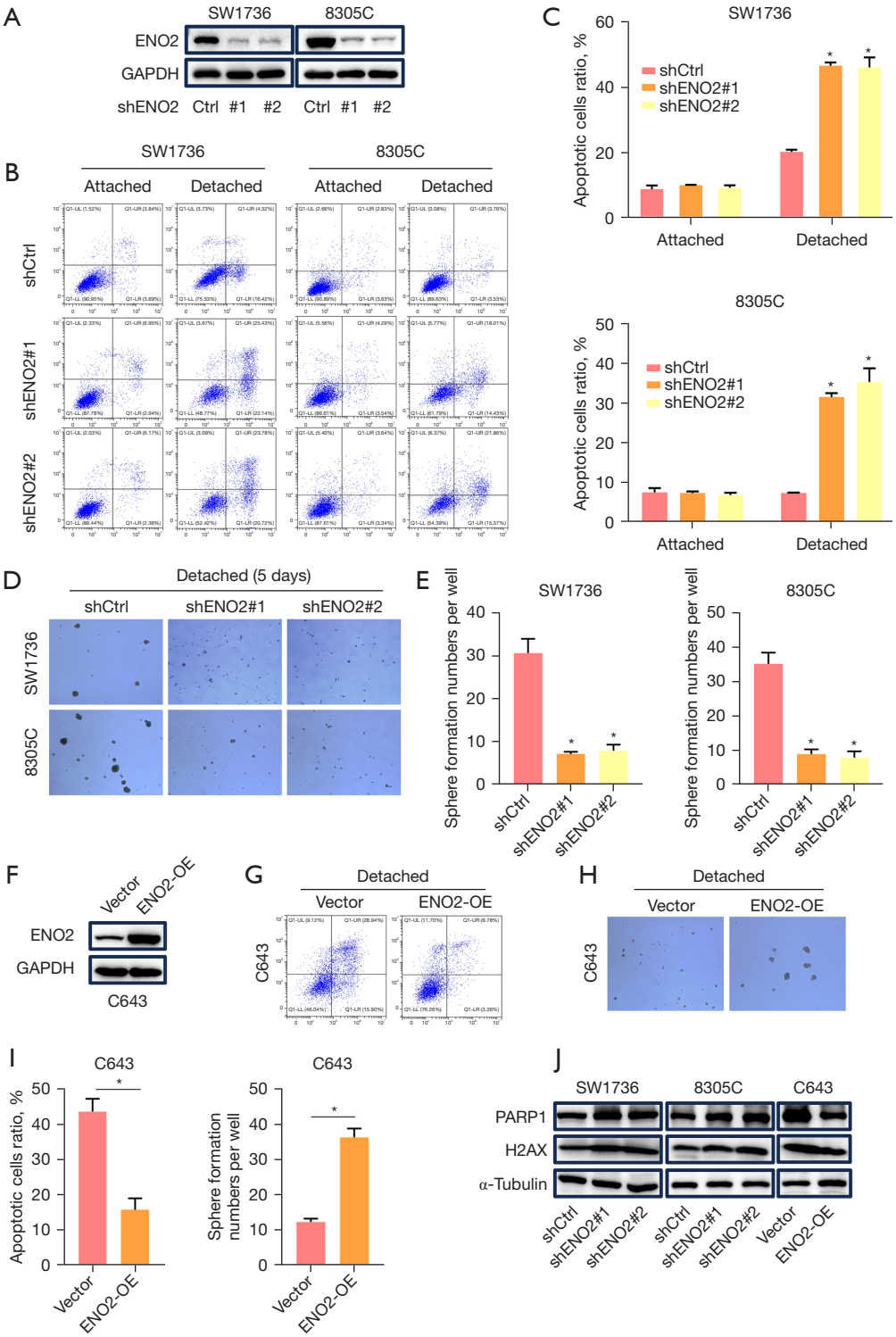

Figure 2 ENO2 regulated anoikis resistance in ATC cells. (A) Western blot analysis of the efficiency of ENO2 knockdown in the SW1736 and 8305C cells. (B,C) Flow cytometry (B) and quantification analysis (C) of cell apoptosis with Annexin V/PI staining in the control and ENO2-knockdown SW1736 and 8305C cells under the attached or detached culture conditions for 48 hours. (D,E) Sphere formation (D) and quantification analysis (E) in the control and ENO2-knockdown SW1736 and 8305C cells under the attached or detached culture conditions for 5 days. The spheres were observed under a microscope. Scale bar, 200 μm. (F) Western blot analysis of the ENO2-overexpression C643 cells. (G-I) Flow cytometry of cell apoptosis (G), sphere formation (H), and associated quantification analysis (I) in the control and ENO2-overexpressing C643 cells. The spheres were observed under a microscope. Scale bar, 200 μm. (J) The SW1736, 8305C, and C643 cells were cultured in the detached culture conditions for 2 days. The western blot analysis showed that PARP1 and H2AX were increased in the ENO2-knockdown cells (SW1736 and 8305C) and decreased in the overexpression-C643 cells. The data in C, E, and I are expressed as the mean ± standard deviation. The P values in C, E, and I were calculated using the two-sided unpaired Student's *t*-test. *, P<0.05. ENO2, enolase 2; ATC, anaplastic thyroid cancer; Annexin V/PI, Annexin V/propidium iodide.

ENO2 knockdown aggravated redox stress induced in the detached culture condition

As a key enzyme in the glycolytic pathway, ENO2 knockdown influenced the oxidative stress levels of ATC cells in detached culture conditions. The ROS levels were found to be significantly elevated in the detached SW1736 and 8305C cells in which ENO2 was knocked down (*Figure 3A*). Additionally, as crucial factors in maintaining the cellular redox balance, NADPH and GSH played vital roles. A further examination of the NADPH expression levels in the detached SW1736 and 8305C cells in which ENO2 was knocked down showed a significant decrease in the NADPH/$NADP^+$ ratio (*Figure 3B*). Additionally, the GSH/GSSG ratio exhibited a similar trend (*Figure 3C*). Further, the application of the antioxidant NAC significantly reversed the effect of ENO2 knockdown on cell apoptosis (*Figure 3D*,*3E*) and a similar effect was observed in the sphere formation assays (*Figure 3F*,*3G*). Therefore, these experiments indicated that the ENO2-mediated redox balance played a crucial protective role in maintaining the anoikis resistance of ATC cells.

STAT1 stimulated the transcription of ENO2

ENO2 has been reported to be overexpressed in various solid tumors, and its regulatory mechanisms include transcriptional regulation. Through transcription factor and relevant binding site prediction in UCSC Genome Browser Home and JASPAR, we found that STAT1 might mediate the transcription of *ENO2*. At the same time, as a crucial transcription factor, STAT1 has been reported to play a significant role in the activation of the glycolytic pathway (32). By combining transcription site prediction in JASPAR, we selected the highest scoring potential binding site (1625–1639) for further validation (*Figure 4A*). The ChIP-qPCR experiments demonstrated the significant enrichment of the binding element in STAT1 immunoprecipitants (*Figure 4B*). Dual-luciferase reporter gene assays indicated that STAT1 overexpression markedly stimulated luciferase activity. However, subsequent experiments with plasmids containing mutations in this binding site (1625–1639) revealed that the effect of STAT1 overexpression was inhibited (*Figure 4C*). Further, after the siRNA-mediated knockdown of STAT1 expression, ENO2 expression was significantly decreased at the mRNA level (*Figure 4D*). Additionally, the protein expression levels of STAT1 exhibited an elevated trend in the SW1736 and 8305C cells in the detached culture condition (*Figure 4E*). Finally, at the protein level, we confirmed that STAT1 knockdown suppressed ENO2 expression (*Figure 4F*). In summary, STAT1 played a vital role in the transcriptional regulation of ENO2 in ATC.

Knockdown of ENO2 inhibited tumor metastasis in vivo

To further explore the effect of ENO2 *in vivo*, shCtrl and shENO2#1 group of 8305C cells were injected into the tail vein of the mice, and lung metastasis was monitored (*Figure 5A*). The knockdown of ENO2 remarkably inhibited the lung metastasis of the 8305C cells (*Figure 5B*). Overall, ENO2 could promote lung metastasis in ATC *in vivo* and might serve as a potential therapeutic target, which is shown in a graphic review (*Figure 5C*).

Discussion

Once detached from the ECM, some cancer cells acquire resistance to anoikis, enabling their survival in blood and lymphatics vessels, thereby facilitating migration to new sites and subsequent metastasis (33,34). In the prevention of tumor metastasis, anoikis resistance represents a key factor contributing to treatment failure (35). Numerous studies have been conducted on the mechanisms of anoikis resistance, and Ras, a small G-protein, was one of the first proteins discovered to prevent cancer cells from undergoing anoikis by activating downstream signaling pathways (36,37). Focal adhesion kinase regulates various pathways, such as PI3K and MAPK, and certain tyrosine kinases like those of the Src family, all of which influence cellular resistance to anoikis (38-40). Protective autophagy has also been reported to be involved in anoikis resistance (41). However, research on ATC regarding anoikis resistance is limited, and the underlying mechanisms remain unclear.

To survive in a harsh environment (e.g., an environment in which the cells are detached from the primary site and facing energy deprivation), tumor cells often undergo adjustments in energy utilization (42-44). The Warburg effect, or aerobic glycolysis, has historically referred to the metabolic reprogramming of malignant cells, and represents the preferred mode by which tumors acquire energy for survival (45,46). This metabolic strategy provides several survival advantages to tumor cells. It allows increased carbon sources for protein synthesis to meet the demands of tumor growth (47). Additionally, by enhancing glycolysis, even under aerobic conditions, it suppresses excessive ROS production, which is vital in inhibiting anoikis. Moreover, the substantial lactate produced via the glycolytic pathway

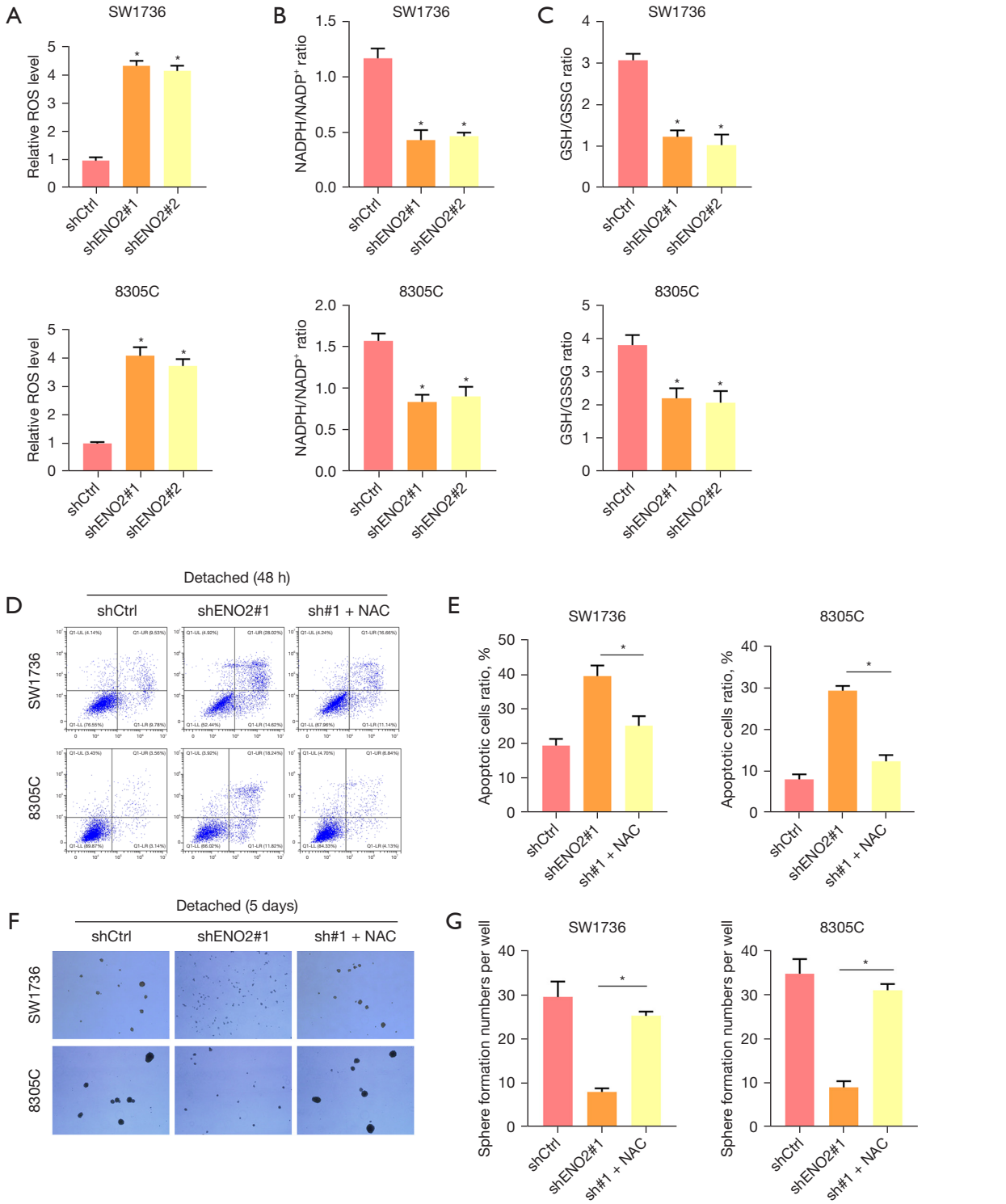

Figure 3 ENO2 knockdown aggravated redox stress induced in the detached culture condition. (A) ROS levels of the control and ENO2-knockdown SW1736 and 8305C cells under the detached culture condition for 24 hours. (B,C) NADPH/NADP+ and GSH/GSSG levels analysis in the control or ENO2-knockdown SW1736 and 8305C cells under the detached culture condition for 24 hours. (D,E) Flow cytometry (D) and quantification analysis (E) of cell apoptosis with Annexin V/PI staining in the detached SW1736 and 8305C cells treated with or without NAC (5 mM) for 48 hours. (F,G) Sphere formation (F) and quantification analysis (G) in the detached SW1736 and 8305C cells treated with or without NAC (5 mM) for 5 days. The spheres were observed under a microscope. Scale bar, 200 μm. The data in A-C, E, and G are expressed as the mean ± standard deviation. The P values in A-C, E, and G were calculated using the two-sided unpaired Student's *t*-test. *, P<0.05. ENO2, enolase 2; ROS, reactive oxygen species; NADPH, nicotinamide adenine dinucleotide phosphate (reduced form); NADP+, nicotinamide adenine dinucleotide phosphate (oxidized form); GSH, glutathione; GSSG, glutathione disulfide; Annexin V/PI, Annexin V/propidium iodide; NAC, N-acetyl cysteine.

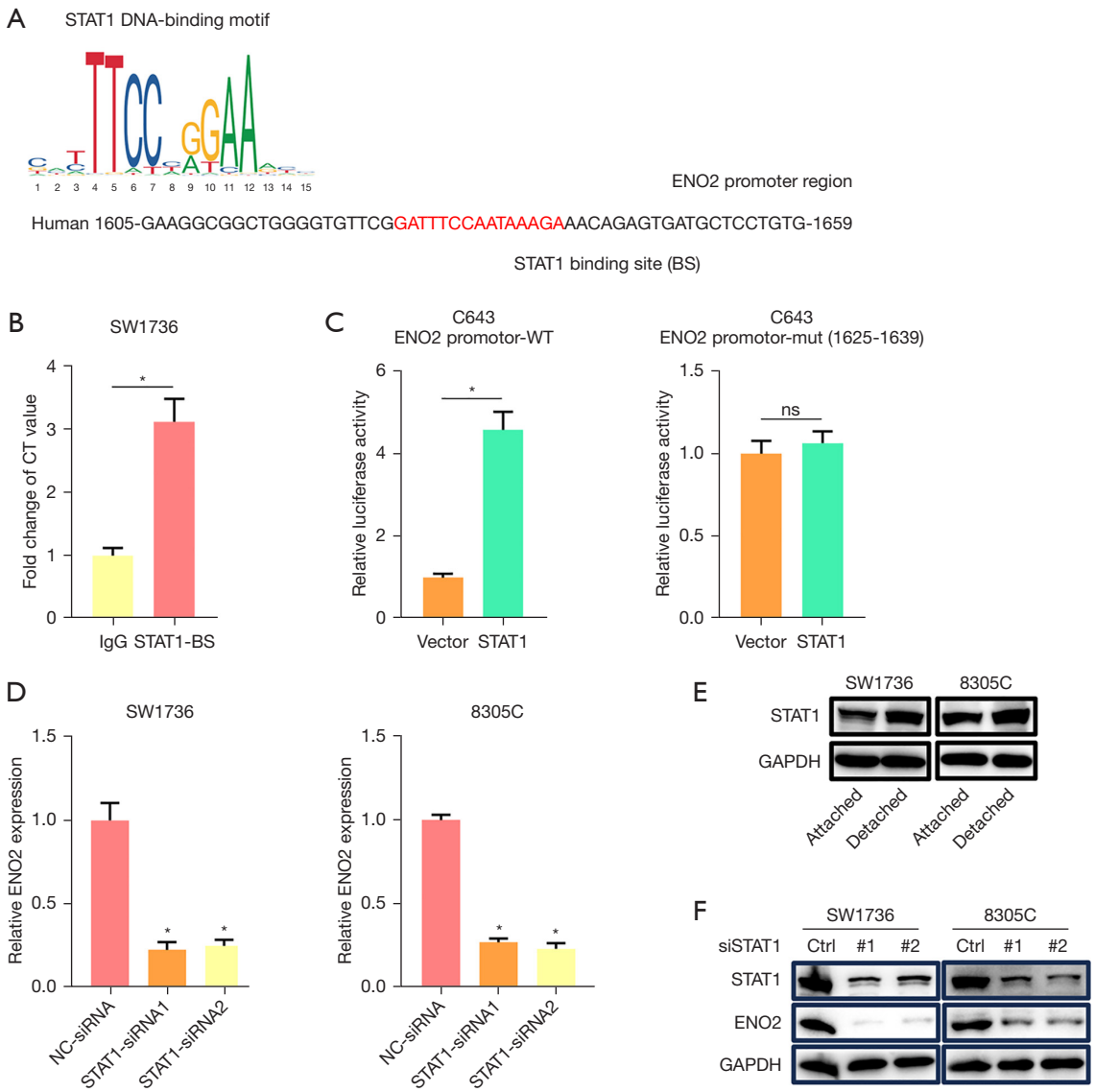

Figure 4 STAT1 stimulated the transcription of ENO2. (A) Diagram displaying the ENO2 promoter containing the STAT1 binding site with prediction in JASPAR. (B) qPCR assay following ChIP analysis indicating the presence of the predicted STAT1 binding site on the ENO2 promoter in the SW1736. (C) Luciferase reporter gene assay of transcriptional activity of each ENO2 promoter (wild-type or mutant) in the C643 cells. (D) qRT-PCR analysis showing the ENO2 expression at the mRNA level after STAT1 knockdown. (E) Western blot analysis showing the expression of STAT1 in the SW1736 and 8305C cells under the detached culture conditions. (F) Western blot analysis showing the ENO2 expression after STAT1 knockdown. The data in B-D are expressed as the mean ± standard deviation. The P values in B-D were calculated using the two-sided unpaired Student's *t*-test. *, P<0.05; ns, not significant. STAT1, signal transducer and activator of transcription 1; ENO2, enolase 2; JASPAR, Joint Analysis of the Structural Parameters of Analytical Representations; CT, computed tomography; ChIP, chromatin immunoprecipitation; qPCR, quantitative polymerase chain reaction; qRT-PCR, quantitative real-time polymerase chain reaction; mRNA, messenger RNA.

contributes to tumor microenvironment acidification, promoting angiogenesis and the renewal of tumor stemness (48,49). Recent studies have also highlighted enhanced lipid metabolism as a distinct metabolic feature in some tumors (11,50,51). For instance, the depletion of LPCAT1, which is responsible for cholesterol synthesis, has been

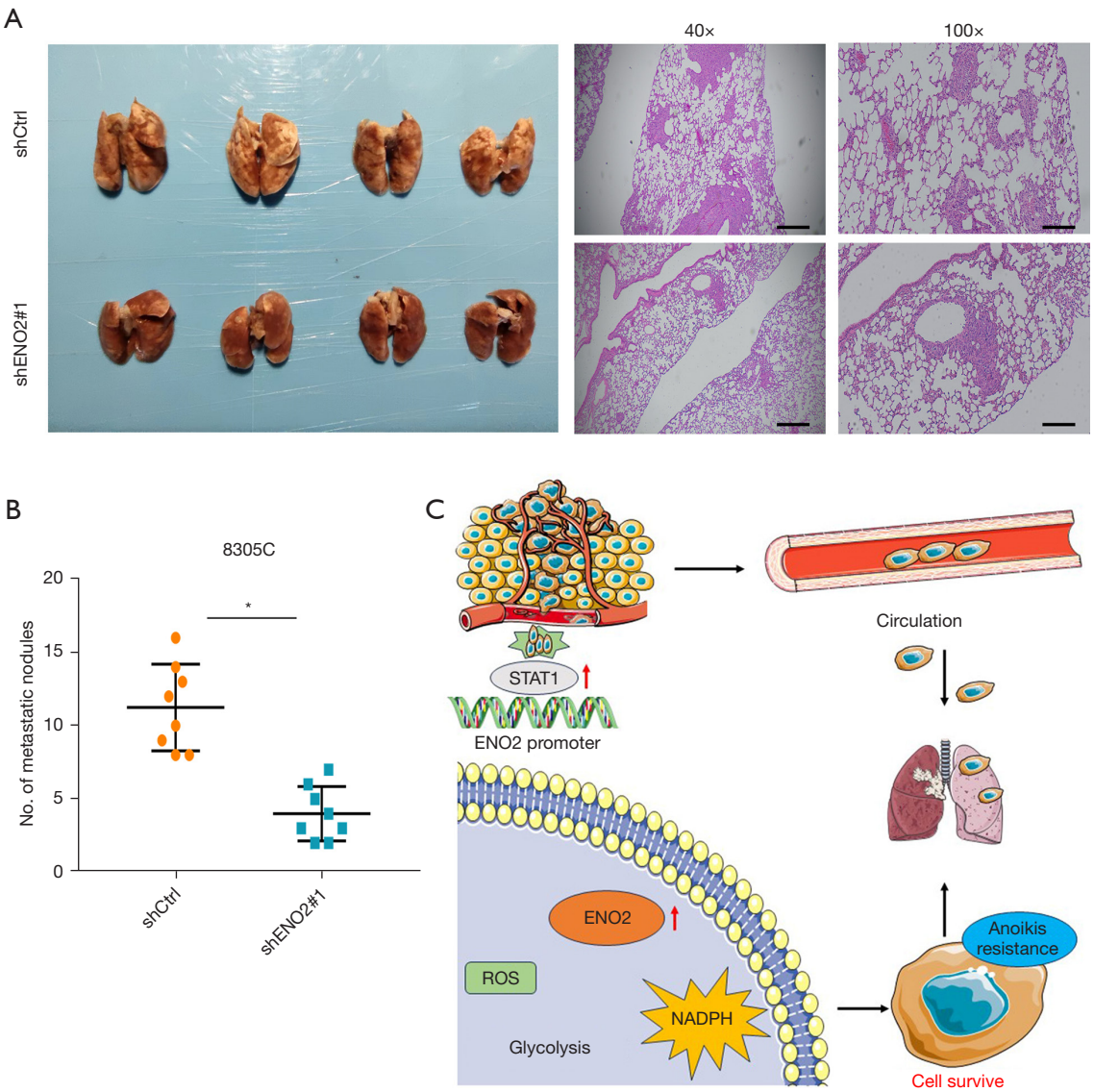

Figure 5 Knockdown of ENO2 inhibited tumor metastasis *in vivo*. (A,B) Representative images and hematoxylin and eosin staining (A) and statistical results (B) of metastatic lung nodules from mice injected via the tail vein with the control and ENO2-knockdown 8305C cells. (C) A graphic review. The P value in B was calculated using the two-sided unpaired Student's *t*-test. *, P<0.05. ENO2, enolase 2; STAT1, Signal Transducer and Activator of Transcription 1; NADPH, nicotinamide adenine dinucleotide phosphate (reduced form); ROS, reactive oxygen species.

proven to inhibit anchorage-independent growth in esophageal squamous cell carcinoma cells (52). Additionally, the upregulation of fatty acid metabolism triggered by CPT1A activation plays a critical role in conferring anoikis resistance in colorectal cancer cells (40). Thus, different tumor cells may rely on distinct energy supplies to resist anoikis, suggesting diverse potential therapeutic targets based on these dependencies.

In this study, the transcriptomic analysis of the three groups of ATC cells revealed that ENO2 was one of the significantly upregulated genes in the detached culture condition. Further, in the tissue samples of ATC patients, the expression of ENO2 was significantly more elevated in the metastatic lymph nodes than in the primary lesions. We hypothesized that the ENO2-mediated glycolysis process might play a crucial role in supplying energy for

anoikis resistance in ATC cells. Previous studies have shown that ENO2 is significantly involved in the development of various tumors (22,28,53), prompting our assumption that regulating ENO2 expression might influence the fate of cells under detached culture conditions. Our *in vitro* experiments demonstrated that the knockdown of ENO2 significantly increased cell apoptosis in the SW1736 and 8305C cells, coupled with a significant decrease in sphere formation. Our *in vivo* experiments also revealed the substantial inhibition of lung metastasis formation in the 8305C cells following ENO2 knockdown. Conversely, the overexpression of ENO2 in the C643 cells suppressed anoikis and increased sphere formation. Therefore, the activation of ENO2-mediated glycolysis process was closely associated with the anoikis resistance in ATC, serving as a significant factor driving distant metastasis in ATC.

To further explore the potential mechanisms behind the upregulation of ENO2 in the anoikis-resistant ATC cells, we focused on changes in ROS production and the maintenance of the redox balance. Considered a double-edged sword for tumor cells, moderate ROS levels facilitate cell proliferation and survival, while excessive ROS levels disrupt the redox microenvironment, potentially inducing tumor cell death and suppressing anoikis resistance. In our *in vitro* experiments, crucial intracellular reducing agents, such as NADPH and GSH, decreased significantly after ENO2 knockdown. Additionally, the reversal of the anoikis phenotype after NAC supplementation further confirmed the pivotal role of the redox balance in the anoikis resistance of ATC cells.

Signal transducer and activator of transcription (STAT) regulates target gene transcription in response to various cytokine signals, participating in modulating tumor cell energy metabolism, tumor progression, and therapy resistance (54). The Warburg effect, a characteristic of tumor cell glucose metabolism, involves glycolysis under aerobic conditions. STAT signaling drives aerobic glycolysis in tumor cells by upregulating the expression of genes such as MYC and HIF (55-57). The increased production of ROS is a critical metabolic feature during the malignant transformation of tumor cells, and its dual role in tumor cells is modulated by STAT (58). Further, STAT itself is regulated by ROS in the process of controlling both pro-carcinogenic and anti-carcinogenic effects (59). Elevated ROS levels promote phosphorylation of JAK2 (pJAK2), leading to the anti-apoptotic action of tumor cells through pJAK2-STAT1 signaling (60). Additionally, STAT1 is involved in the generation of ROS scavenger NQO1. Thus, inhibiting STAT1 signaling weakens NQO1 activity, elevates ROS levels, and induces tumor cell death (61). Meanwhile, STAT5 has been reported to play an important role in tumor progression and the activation of the glycolytic pathway (62). Further, a study indicates that STAT3 enhances the transcription of HK2 to modulate physiological responses under hypoxia (63), where HK2 is a crucial enzyme in the glycolytic pathway. Our study identified the role of STAT1 in the enhanced transcriptional regulation of ENO2, further elucidating the energy metabolism mechanism during hypoxia or anoikis resistance in tumors, presenting a potential target for future therapies in ATC.

We initiated our research by investigating the activation of the glycolytic pathway in ATC cells and preliminarily explored the mechanisms of anoikis resistance in ATC. Anoikis is a programmed cell death, which occurs when tumor cells detach from the ECM or neighboring cells. As a crucial component of the tumor microenvironment, the ECM undoubtedly plays a significant role in the process of anoikis resistance in ATC. In our further studies, we will focus on the crosstalk between the tumor microenvironment and ATC cells during anoikis resistance. Simultaneously, we believe that investigating and developing potential clinical interventions targeting anoikis resistance holds significant promise for improving the treatment and prognosis of ATC. This study had some limitations. Due to the lack of fresh ATC samples and matched metastatic tissues, we were unable to conduct the transcriptomic sequencing of the tissue samples. Additionally, we did not perform experiments involving therapeutic inhibitors targeting the STAT1 and ENO2 signaling pathways. Therefore, in our next study, we intend to validate the biomarker potential of ENO2 in a large cohort of ATC patients from FUSCC. Additionally, we also intend to validate the STAT1/ENO2-mediated anoikis resistance in more comprehensive *in vivo* models and explore targeted drug inhibitors.

Conclusions

This study showed that the glycolytic pathway is significantly upregulated in ATC cells under detached culture conditions, and thus established that it plays a crucial role in promoting anoikis resistance. Among several upregulated genes, the stable expression of ENO2 and the maintenance of the redox balance play pivotal roles in facilitating the anoikis resistance of ATC cells. Additionally, the transcriptional regulation between STAT1 and ENO2 further confirmed the involvement of the STAT family in regulating aerobic

glycolysis and the Warburg effect. Hence, metabolic reprogramming mediated by ENO2 could be modulated to be a potential therapeutic target for ATC.

Acknowledgments

We are very grateful to the research platform of Fudan University Cancer Hospital. We are grateful to Dr. Wang Xing from Shanghai Jiao Tong University for technical support.
Funding: The study was supported by the Science and Technology Commission of Shanghai Municipality (No. 22Y21900100 to Y.W.).

Footnote

Reporting Checklist: The authors have completed the ARRIVE and MDAR reporting checklists. Available at https://gs.amegroups.com/article/view/10.21037/gs-24-44/rc

Data Sharing Statement: Available at https://gs.amegroups.com/article/view/10.21037/gs-24-44/dss

Peer Review File: Available at https://gs.amegroups.com/article/view/10.21037/gs-24-44/prf

Conflicts of Interest: All authors have completed the ICMJE uniform disclosure form (available at https://gs.amegroups.com/article/view/10.21037/gs-24-44/coif). The authors have no conflicts of interest to declare.

Ethical Statement: The authors are accountable for all aspects of the work in ensuring that questions related to the accuracy or integrity of any part of the work are appropriately investigated and resolved. The study was conducted in accordance with the Declaration of Helsinki (as revised in 2013). The study was approved by the Ethics Committee of Fudan University Shanghai Cancer Center (No. 050432-4-2108) and informed consent was taken from all the patients. Animal experiments were performed under a project license (No. FUSCC-IACUC-S2023-0429) granted by Experimental Animal Welfare Ethics Committee of Fudan University Shanghai Cancer Center, in compliance with institutional guidelines for the care and use of animals.

References

1. Haddad RI, Nasr C, Bischoff L, et al. NCCN Guidelines Insights: Thyroid Carcinoma, Version 2.2018. J Natl Compr Canc Netw 2018;16:1429-40.
2. Lamartina L, Hadoux J. Randomised controlled trials are feasible in anaplastic thyroid cancer. Lancet Oncol 2023;24:119-21.
3. Lu L, Wang JR, Henderson YC, et al. Anaplastic transformation in thyroid cancer revealed by single-cell transcriptomics. J Clin Invest 2023;133:e169653.
4. Fallahi P, Ferrari SM, Galdiero MR, et al. Molecular targets of tyrosine kinase inhibitors in thyroid cancer. Semin Cancer Biol 2022;79:180-96.
5. Ibrahimpasic T, Ghossein R, Shah JP, et al. Poorly Differentiated Carcinoma of the Thyroid Gland: Current Status and Future Prospects. Thyroid 2019;29:311-21.
6. Rao SN, Smallridge RC. Anaplastic thyroid cancer: An update. Best Pract Res Clin Endocrinol Metab 2023;37:101678.
7. Hofmann MC, Kunnimalaiyaan M, Wang JR, et al. Molecular mechanisms of resistance to kinase inhibitors and redifferentiation in thyroid cancers. Endocr Relat Cancer 2022;29:R173-90.
8. Zhang L, Feng Q, Wang J, et al. Molecular basis and targeted therapy in thyroid cancer: Progress and opportunities. Biochim Biophys Acta Rev Cancer 2023;1878:188928.
9. Ji H, Hu C, Yang X, et al. Lymph node metastasis in cancer progression: molecular mechanisms, clinical significance and therapeutic interventions. Signal Transduct Target Ther 2023;8:367.
10. Zhan Q, Liu B, Situ X, et al. New insights into the correlations between circulating tumor cells and target organ metastasis. Signal Transduct Target Ther 2023;8:465.
11. Tian T, Lu Y, Lin J, et al. CPT1A promotes anoikis resistance in esophageal squamous cell carcinoma via redox homeostasis. Redox Biol 2022;58:102544.
12. Weems AD, Welf ES, Driscoll MK, et al. Blebs promote cell survival by assembling oncogenic signalling hubs. Nature 2023;615:517-25.

13. Zhang HF, Hughes CS, Li W, et al. Proteomic Screens for Suppressors of Anoikis Identify IL1RAP as a Promising Surface Target in Ewing Sarcoma. Cancer Discov 2021;11:2884-903.
14. Wang Y, Xie C, Su Y. A novel anoikis-related gene signature to predict the prognosis, immune infiltration, and therapeutic outcome of lung adenocarcinoma. J Thorac Dis 2023;15:1335-52.
15. Huh HD, Sub Y, Oh J, et al. Reprogramming anchorage dependency by adherent-to-suspension transition promotes metastatic dissemination. Mol Cancer 2023;22:63.
16. Zhang C, Wang Y, Zhen Z, et al. mTORC1 Mediates Biphasic Mechano-Response to Orchestrate Adhesion-Dependent Cell Growth and Anoikis Resistance. Adv Sci (Weinh) 2024;11:e2307206.
17. Li X, Yang Y, Zhang B, et al. Lactate metabolism in human health and disease. Signal Transduct Target Ther 2022;7:305.
18. Hsu PP, Sabatini DM. Cancer cell metabolism: Warburg and beyond. Cell 2008;134:703-7.
19. Boese AC, Kang S. Mitochondrial metabolism-mediated redox regulation in cancer progression. Redox Biol 2021;42:101870.
20. Kamarajugadda S, Stemboroski L, Cai Q, et al. Glucose oxidation modulates anoikis and tumor metastasis. Mol Cell Biol 2012;32:1893-907.
21. De Vitis C, Battaglia AM, Pallocca M, et al. ALDOC- and ENO2- driven glucose metabolism sustains 3D tumor spheroids growth regardless of nutrient environmental conditions: a multi-omics analysis. J Exp Clin Cancer Res 2023;42:69.
22. Wang C, Huang M, Lin Y, et al. ENO2-derived phosphoenolpyruvate functions as an endogenous inhibitor of HDAC1 and confers resistance to antiangiogenic therapy. Nat Metab 2023;5:1765-86.
23. Tian Z, Liang C, Zhang Z, et al. Prognostic value of neuron-specific enolase for small cell lung cancer: a systematic review and meta-analysis. World J Surg Oncol 2020;18:116.
24. Tang Y, Zhang H, Chen L, et al. Identification of Hypoxia-Related Prognostic Signature and Competing Endogenous RNA Regulatory Axes in Hepatocellular Carcinoma. Int J Mol Sci 2022;23:13590.
25. Kim J, Jin H, Zhao JC, et al. FOXA1 inhibits prostate cancer neuroendocrine differentiation. Oncogene 2017;36:4072-80.
26. Zheng Y, Wu C, Yang J, et al. Insulin-like growth factor 1-induced enolase 2 deacetylation by HDAC3 promotes metastasis of pancreatic cancer. Signal Transduct Target Ther 2020;5:53.
27. Wang Q, Chen C, Ding Q, et al. METTL3-mediated m(6)A modification of HDGF mRNA promotes gastric cancer progression and has prognostic significance. Gut 2020;69:1193-205.
28. Lv C, Yu H, Wang K, et al. ENO2 Promotes Colorectal Cancer Metastasis by Interacting with the LncRNA CYTOR and Activating YAP1-Induced EMT. Cells 2022;11:2363.
29. Brown CW, Amante JJ, Mercurio AM. Cell clustering mediated by the adhesion protein PVRL4 is necessary for α6β4 integrin-promoted ferroptosis resistance in matrix-detached cells. J Biol Chem 2018;293:12741-8.
30. Huang Q, Li S, Hu X, et al. Shear stress activates ATOH8 via autocrine VEGF promoting glycolysis dependent-survival of colorectal cancer cells in the circulation. J Exp Clin Cancer Res 2020;39:25.
31. Jin L, Chun J, Pan C, et al. Phosphorylation-mediated activation of LDHA promotes cancer cell invasion and tumour metastasis. Oncogene 2017;36:3797-806.
32. Liu P, Zhou Y, Chen C, et al. Lysophosphatidylcholine facilitates the pathogenesis of psoriasis through activating keratinocytes and T cells differentiation via glycolysis. J Eur Acad Dermatol Venereol 2023;37:1344-60.
33. Kim K, Huang H, Parida PK, et al. Cell Competition Shapes Metastatic Latency and Relapse. Cancer Discov 2023;13:85-97.
34. Endo H, Owada S, Inagaki Y, et al. Metabolic reprogramming sustains cancer cell survival following extracellular matrix detachment. Redox Biol 2020;36:101643.
35. Yuan Z, Li Y, Zhang S, et al. Extracellular matrix remodeling in tumor progression and immune escape: from mechanisms to treatments. Mol Cancer 2023;22:48.
36. Eckert LB, Repasky GA, Ulkü AS, et al. Involvement of Ras activation in human breast cancer cell signaling, invasion, and anoikis. Cancer Res 2004;64:4585-92.
37. Debnath J. p66(Shc) and Ras: controlling anoikis from the inside-out. Oncogene 2010;29:5556-8.
38. Stulpinas A, Uzusienis T, Imbrasaite A, et al. Cell-cell and cell-substratum contacts in the regulation of MAPK and Akt signalling: Importance in therapy, biopharmacy and bioproduction. Cell Signal 2021;84:110034.
39. Li K, Zhao G, Ao J, et al. ZNF32 induces anoikis resistance through maintaining redox homeostasis and activating Src/FAK signaling in hepatocellular carcinoma. Cancer Lett 2019;442:271-8.
40. Wang YN, Zeng ZL, Lu J, et al. CPT1A-mediated fatty acid oxidation promotes colorectal cancer cell metastasis by inhibiting anoikis. Oncogene 2018;37:6025-40.

41. Yu Y, Song Y, Cheng L, et al. CircCEMIP promotes anoikis-resistance by enhancing protective autophagy in prostate cancer cells. J Exp Clin Cancer Res 2022;41:188.
42. Xia P, Zhang H, Lu H, et al. METTL5 stabilizes c-Myc by facilitating USP5 translation to reprogram glucose metabolism and promote hepatocellular carcinoma progression. Cancer Commun (Lond) 2023;43:338-64.
43. Wu D, Yang Y, Hou Y, et al. Increased mitochondrial fission drives the reprogramming of fatty acid metabolism in hepatocellular carcinoma cells through suppression of Sirtuin 1. Cancer Commun (Lond) 2022;42:37-55.
44. Liu X, Qin H, Zhang L, et al. Hyperoxia induces glucose metabolism reprogramming and intracellular acidification by suppressing MYC/MCT1 axis in lung cancer. Redox Biol 2023;61:102647.
45. Li M, Yang Y, Xiong L, et al. Metabolism, metabolites, and macrophages in cancer. J Hematol Oncol 2023;16:80.
46. Jing Z, Liu Q, He X, et al. NCAPD3 enhances Warburg effect through c-myc and E2F1 and promotes the occurrence and progression of colorectal cancer. J Exp Clin Cancer Res 2022;41:198.
47. Liberti MV, Allen AE, Ramesh V, et al. Evolved resistance to partial GAPDH inhibition results in loss of the Warburg effect and in a different state of glycolysis. J Biol Chem 2020;295:111-24.
48. Rastogi S, Mishra SS, Arora MK, et al. Lactate acidosis and simultaneous recruitment of TGF-β leads to alter plasticity of hypoxic cancer cells in tumor microenvironment. Pharmacol Ther 2023;250:108519.
49. Liang B, Jiang Y, Song S, et al. ASPP2 suppresses tumour growth and stemness characteristics in HCC by inhibiting Warburg effect via WNT/β-catenin/HK2 axis. J Cell Mol Med 2023;27:659-71.
50. Mah CY, Nguyen ADT, Niijima T, et al. Peroxisomal β-oxidation enzyme, DECR2, regulates lipid metabolism and promotes treatment resistance in advanced prostate cancer. Br J Cancer 2024. [Epub ahead of print]. doi: 10.1038/s41416-023-02557-8.
51. Vogel FCE, Chaves-Filho AB, Schulze A. Lipids as mediators of cancer progression and metastasis. Nat Cancer 2024;5:16-29.
52. Tao M, Luo J, Gu T, et al. LPCAT1 reprogramming cholesterol metabolism promotes the progression of esophageal squamous cell carcinoma. Cell Death Dis 2021;12:845.
53. Gao L, Yang F, Tang D, et al. Mediation of PKM2-dependent glycolytic and non-glycolytic pathways by ENO2 in head and neck cancer development. J Exp Clin Cancer Res 2023;42:1.
54. Li YJ, Zhang C, Martincuks A, et al. STAT proteins in cancer: orchestration of metabolism. Nat Rev Cancer 2023;23:115-34.
55. Valle-Mendiola A, Soto-Cruz I. Energy Metabolism in Cancer: The Roles of STAT3 and STAT5 in the Regulation of Metabolism-Related Genes. Cancers (Basel) 2020;12:124.
56. Huang L, Liu D, Wang N, et al. Integrated genomic analysis identifies deregulated JAK/STAT-MYC-biosynthesis axis in aggressive NK-cell leukemia. Cell Res 2018;28:172-86.
57. Choi KM, Kim JJ, Yoo J, et al. The interferon-inducible protein viperin controls cancer metabolic reprogramming to enhance cancer progression. J Clin Invest 2022;132:e157302.
58. Zhou J, Li T, Chen H, et al. ADAMTS10 inhibits aggressiveness via JAK/STAT/c-MYC pathway and reprograms macrophage to create an anti-malignant microenvironment in gastric cancer. Gastric Cancer 2022;25:1002-16.
59. Pratheeshkumar P, Son YO, Divya SP, et al. Luteolin inhibits Cr(VI)-induced malignant cell transformation of human lung epithelial cells by targeting ROS mediated multiple cell signaling pathways. Toxicol Appl Pharmacol 2014;281:230-41.
60. Liu J, Qu L, Meng L, et al. Topoisomerase inhibitors promote cancer cell motility via ROS-mediated activation of JAK2-STAT1-CXCL1 pathway. J Exp Clin Cancer Res 2019;38:370.
61. Totten SP, Im YK, Cepeda Cañedo E, et al. STAT1 potentiates oxidative stress revealing a targetable vulnerability that increases phenformin efficacy in breast cancer. Nat Commun 2021;12:3299.
62. Li SB, Liu YY, Yuan L, et al. Autocrine INSL5 promotes tumor progression and glycolysis via activation of STAT5 signaling. EMBO Mol Med 2020;12:e12050.
63. Dinarello A, Betto RM, Diamante L, et al. STAT3 and HIF1α cooperatively mediate the transcriptional and physiological responses to hypoxia. Cell Death Discov 2023;9:226.

Cite this article as: Zhang Y, Ji X, Wang Y. ENO2 promotes anoikis resistance in anaplastic thyroid cancer by maintaining redox homeostasis. Gland Surg 2024;13(2):209-224. doi: 10.21037/gs-24-44